

Negative reflection of elastic waves in complex environments

Benoît Gérardin, Jérôme Laurent, François Legrand, Claire Prada, and Alexandre Aubry*

ESPCI Paris, PSL Research University, CNRS, Univ Paris Diderot, Sorbonne Paris Cité,
Institut Langevin, UMR 7587, 1 rue Jussieu, F-75005 Paris, France

(Dated: July 18, 2022)

A negative reflecting mirror converts a wave of positive phase velocity into its negative counterpart and vice versa. Whatever the complexity of the propagation medium, the negatively reflected wave field focuses back towards the initial source location, thereby mimicking a phase conjugation operation while being a fully passive process. In this paper, we experimentally demonstrate this phenomenon with elastic waves in a 2D billiard and in a disordered plate by means of laser interferometry. These proof-of-concept experiments show that negative reflection can be a tool of choice for the control and focusing of waves in complex environments.

Controlling the propagation of acoustic or electromagnetic waves, is of fundamental interest for many applications ranging from imaging the living and detecting hazardous components, to information processing and structural health monitoring. In the past decades, there has been many proposals in this regards, which can be separated within two approaches. On the one hand, the wave fields can be tamed in order to take advantage of the complexity of propagation media, for instance, to focus waves or image various objects. This is realized in the temporal domain using time reversal (TR) mirrors [1–3] or in the spatial domain using phase conjugation (PC) [4–6] and wave front shaping techniques [7] developed in optics. On the other hand, one can force waves along desired paths through a careful design of man-made materials. This can be achieved using metamaterials, an arrangement of tailored sub-wavelength building blocks from which the material gains its unusual properties [8–10]. The advent of such structures has given rise to fascinating concepts such as negative refraction [11–13], transformation optics [14, 15] or metasurfaces [16]. Although the concepts of TR and negative refraction have been developed in an independent fashion, they are intimately linked processes [17, 18].

In this Letter, we want to push forward this analogy by investigating the negative reflection (NR) phenomenon. A NR mirror is an interface at which light or sound is retro-reflected. There is a strong similarity with a PC mirror. In a PC experiment, if the incident wave is divergent, the PC wave is converging [Fig. 1(a)]. It follows the same path as the incident wave but in an opposite way. The incident wave vectors are reversed and the PC wave back-focuses exactly on the source location. Let us now consider a NR mirror and an incident wave with a Poynting vector, Π_i , and a wave vector, \mathbf{k}_i , pointing in the same direction (*i.e* with a positive phase velocity) [see Fig. 1(b,c)]. The NR mirror gives rise to a reflected wave of negative phase velocity, *i.e* with a Poynting vector, Π_r , and a wave vector, \mathbf{k}_r , of opposite direction [see Fig. 1(b,c)]. By virtue of the Snell-Descartes law, the incident and reflected wave vectors are strictly identical ($\mathbf{k}_r = \mathbf{k}_i$) but their Poynting vectors shall be in opposite directions ($\Pi_r = -\Pi_i$) [Fig. 1(b)]. If the incident wave is divergent, the NR wave back-converges towards the initial source position. We thus recover a similar effect as in PC, although the reflected wave vectors in each case are in oppo-

site directions [Fig. 1(a,c)]. The PC concept and its temporal equivalent, TR, have shown to be particularly powerful in reverberating or through inhomogeneous media [1, 19, 20]. If the phase accumulated by the waves following each scattering path is reversed, the PC waves re-accumulate the same phase during their trip back due to spatial reciprocity. They finally sum up coherently at the initial source location. This has led to spectacular focusing experiments in acoustics and optics (see Ref. [7] and references therein). Any scattering or reverberating medium can become a lens if the incident wave is properly designed by a PC process. In this Letter, we show how NR can provide similar focusing abilities in complex environments.

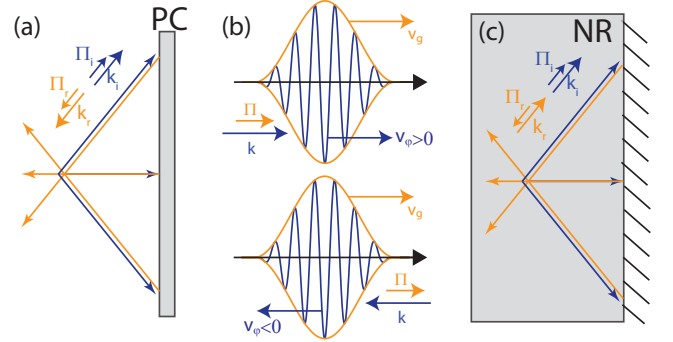


FIG. 1: Analogy between phase conjugation and negative reflection. (a) A PC mirror has the property to reverse both the propagation direction and the phase of an incident wave field. A backward wave is then produced and back-focuses on the source. (b) NR requires the coexistence of positive and negative phase velocity modes. A wave packet exhibiting a positive/negative phase velocity, v_ϕ , is associated with parallel/antiparallel wave and Poynting vectors, respectively. (c) A NR mirror converts an incident wave of phase velocity v_ϕ into a wave of opposite phase velocity $-v_\phi$. The conservation of the parallel momentum at its boundary implies that the incident and reflected wave vectors are strictly identical ($\mathbf{k}_i = \mathbf{k}_r$) while their Poynting vectors are in opposite direction ($\Pi_i = -\Pi_r$). The NR wave thus back-focuses on the initial source location.

NR can occur in a medium that can simultaneously support waves with positive and negative phase velocities. This may happen in chiral metamaterials [21, 22], photonic crystals [23], or in graphene [24], where the pseudo-spin of an electron controls the phase evolution. Apparent negative reflection can

also be induced by a diffraction grating or a metasurface [25] but, in that case, the underlying mechanism does not involve any phase reversal. In this paper, we will explore the NR of elastic waves propagating in a plate. An elastic plate actually support an ensemble of modes, the so-called Lamb waves, which exhibit complex dispersion properties. In particular, some Lamb modes, often referred to as backward propagating modes, naturally display a negative phase velocity [26–29]. This peculiar property has been taken advantage of to achieve negative refraction [30, 31] through mode conversion between forward and backward propagating modes (or vice versa) at a step-like thickness discontinuity. This conversion from forward to backward Lamb waves also occurs at a simple free edge of an elastic plate, giving rise to NR [32–34]. In this Letter, this phenomenon is investigated in complex environments by means of laser interferometry [see Fig. 2]. Whereas the reflection of waves at the boundaries of a cavity or by a random distribution of scatterers usually induces a fully random speckle wave field, NR will be shown to give rise to a purely deterministic wave field: the PC replica of the incident wave.

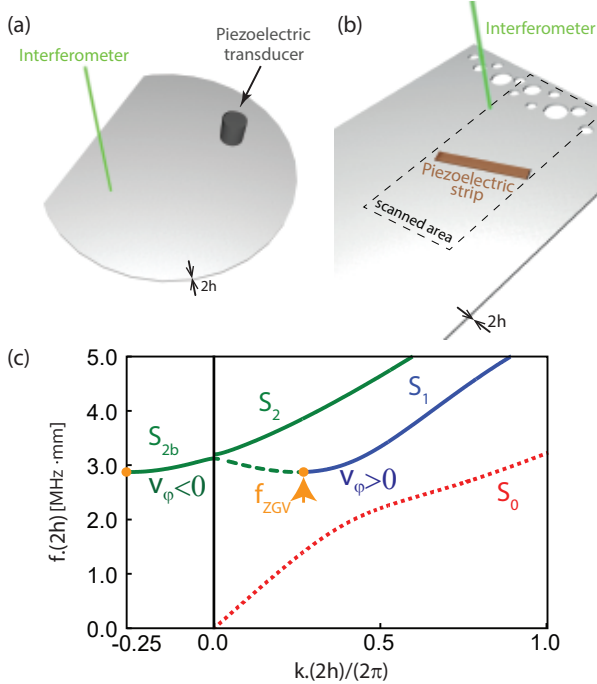


FIG. 2: Experimental configuration. (a) Lamb modes are generated in a Duralumin plate of thickness $2h = 1.5$ mm by a 7 mm-diameter transducer. The Duralumin plate is here a 80 mm-diameter truncated chaotic billiard. (b) Lamb modes are excited in a disordered Duralumin plate of dimension $2h = 2$ mm by a piezoelectric strip. In each case (a)-(b), the normal component of the plate vibration is measured with an interferometric optical probe, mounted on a 2D translation stage. (c) Dispersion curves of the first propagating symmetrical Lamb modes in a Duralumin plate computed from the Rayleigh Lamb equation [35].

We study here the propagation of elastic waves across a Duralumin plate (aluminium alloy), with a density $\rho = 2790$ kg/m³, a longitudinal wave velocity $c_L = 6400$ m.s⁻¹, and a transverse wave velocity $c_T = 3120$ m.s⁻¹. Lamb waves are elastic waves whose particle motion lies in the sagittal plane that contains the direction of wave propagation and the plate normal. Whereas an infinite medium supports two longitudinal and transverse modes traveling at unique velocities, plates support two infinite sets of Lamb wave modes. The deformation induced by these modes can be either symmetric or antisymmetric with respect to the median plane. In this paper, we specifically focus on the symmetric modes. Their dispersion curves in Duralumin are displayed in Fig. 2(c). The symmetric zero-order mode S_0 is the extensional mode of the plate. It exhibits free propagation to zero frequency, whereas the higher order modes admit a cut-off frequency. The dispersion branch S_1 displays several crucial features. As illustrated by Fig. 2(c), its repulsion with the S_2 -mode gives rise to a zero-group velocity (ZGV) point (f_{ZGV}, k_{ZGV}) [36, 37]. In the case of Duralumin, $f_{ZGV} \times 2h = 2.86$ MHz·mm and $k_{ZGV} \times 2h/(2\pi) = 0.26$, with $2h$ the plate thickness. From the ZGV resonance f_{ZGV} to the cut-off frequency, there is a coexistence between a negative phase velocity (backward) mode, referred to as S_{2b} in the literature, and the positive phase velocity (forward) mode S_1 [28]. A remarkable feature is the perfect conversion between these two modes at a free edge in the vicinity of the ZGV-point [34]. It arises from the equality of their wave number at the ZGV-point. This implies that these two modes are associated with similar stress-displacement fields and only differ by their opposite Poynting vectors. As a consequence, the stress-free boundary condition at the edge of the plate can be satisfied with a simple combination of S_1 and S_{2b} modes stress field, leading to a reflection coefficient $r = -1$. This peculiar property holds over the whole angular spectrum close to the ZGV-point. A free edge then acts as a nearly perfect NR mirror for the S_1 and S_{2b} modes [34].

This striking behavior is first investigated in an elastic chaotic cavity [see Fig. 2(a)]. The Duralumin plate is here a 80 mm-diameter truncated chaotic billiard. The plate thickness is $2h = 1.5$ mm. The ZGV-point occurs at $f_{ZGV} = 1.91$ MHz and $k_{ZGV} = 1.06$ mm⁻¹. The ultrasound source consists in a 7 mm-diameter piezo-electric transducer placed on top of the plate. Such a transducer allows to selectively excite the S_{2b} -mode [34]. A 10 μ s chirp signal spanning the frequency range 1.8 – 2.0 MHz is sent to the transducer which generates an incident wave front in the plate. The out-of-plane component of the local vibration is detected on the other side of the plate by a two-wave mixing photorefractive interferometer. Signals recorded by the optical probe (Bossa Nova Tempo 1D) are fed into a digital sampling oscilloscope and transferred to a computer. The corresponding wave field is measured over a grid of points that maps the plate surface with a pitch of 1 mm and over a time length of 1 ms. A discrete Fourier transform of the recorded signals is first performed over the temporal domain. The S_{2b} and S_1 contributions are then separated with spatial

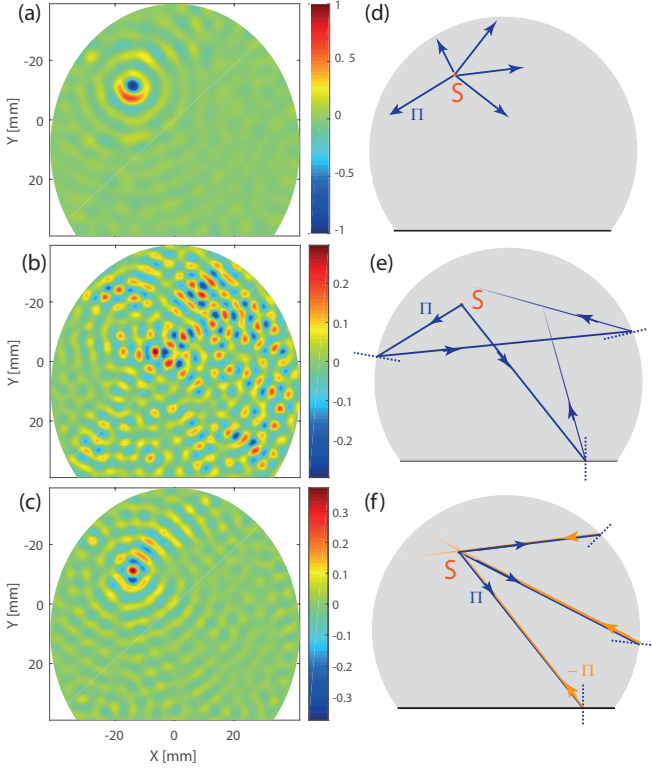


FIG. 3: Negative reflection in the truncated billiard. (a) Incident wave field associated with the excited S_{2b} -mode at frequency $f = 1.91$ MHz. (b) Reflected wave field associated with the S_1 -mode at frequency $f = 1.92$ MHz. (c) NR wave field associated with the S_1 -mode at frequency $f = 1.91$ MHz. (d,e,f) Ray path trajectories involved in (a,b,c), respectively.

low and high pass filters, respectively, with a cut-off at k_{ZGV} [38]. Figure 3(a) shows the incident S_{2b} wave field in the vicinity of the ZGV frequency ($f = 1.91$ MHz). Not surprisingly, it displays divergent cylindrical wave fronts centered around the transducer location. Figures 3(b) and (c) show the reflected S_1 wave field at $f = 1.92$ MHz and $f = 1.91$ MHz, respectively. The first frequency is well above the ZGV-point displayed in Fig. 2(c). There is a clear mismatch between the S_1 and S_{2b} wave numbers: $k_1 = 1.26 \text{ mm}^{-1}$ and $k_{2b} = 0.86 \text{ mm}^{-1}$, respectively [38]. This explains the random feature displayed by the reflected wave field in Fig. 3(b), which is characteristic of a chaotic cavity [Fig. 3(e)]. In the vicinity of the ZGV frequency ($f = 1.91$ MHz), the wave numbers of S_1 and S_{2b} almost coincide: $k_1 = 1.145 \text{ mm}^{-1}$ and $k_{2b} = 0.975 \text{ mm}^{-1}$ [38]. As a consequence, NR gives rise to a cylindrical wave front that converges back towards the initial source location [Figs. 3(c,f)], thus mimicking a PC experiment. Note that the NR wave field [Fig. 3(e)] is out-of-phase compared to the incident wave front [Fig. 3(a)], thereby confirming the theoretical prediction of a reflection coefficient, $r = -1$, between the S_1 and S_{2b} modes at the ZGV-point [34]. As for a TR experiment in a cavity, the size of the focal spot originating from the NR process is limited to a half-wavelength [20]. This can

be interpreted in terms of the diffraction limit and the loss of the evanescent components.

The dynamics of the NR process can be revealed by performing a discrete Fourier transform of the recorded signals over apodized time windows. The corresponding snapshots of the wave propagation versus time are displayed in Fig. 4. The top and bottom panels show the temporal evolution of the S_{2b} and S_1 modes, respectively, at the central frequency $f = 1.91$ MHz. At short time ($t = 0 - 25 \mu\text{s}$), the S_{2b} -mode is largely predominant confirming its selective excitation by the transducer. The incident wave front then propagates across the cavity and finally vanishes when it reaches the cavity boundary. The residual S_{2b} random wave field observed at long times of flight ($t = 200 - 400 \mu\text{s}$) can be explained by the spurious reflections undergone by the NR wave field when it converges back to the transducer. Fig. 4(b) displays the time evolution of the S_1 -mode. As soon as the incident S_{2b} -mode reaches the cavity boundary, it is converted into the NR S_1 -mode. As in a PC or TR experiment, the NR wave field focuses back on the source location. A nice focus is obtained for instance over the time range $t = 0 - 200 \mu\text{s}$. Beyond that time, we observe a progressive degradation of the focal spot. Longer NR paths are actually more sensitive to the slight mismatch between the wave numbers k_1 and k_{2b} in the vicinity of the ZGV-point [38]. Figures 3 and 4 provide a nice illustration of the NR phenomenon. Whatever the chaotic feature of the environment, the incident wave field is re-created, but traveling backward, retracing its passage through the medium and focusing back to the source location. However, unlike TR or PC, a NR mirror is fully passive. No energy is injected into the system through a TR mirror or a nonlinear wave mixing process.

Following the demonstration of the NR phenomenon in a cavity, we now address the more challenging case of a diffusive layer. The experiment is depicted in Fig. 2(b). The system under study is now a plate of thickness $2h \sim 2 \text{ mm}$ for which the ZGV-point occurs at $f_{ZGV} = 1.41 \text{ MHz}$ and $k_{ZGV} = 0.89 \text{ mm}^{-1}$. Randomness is introduced by drilling circular holes with diameters ranging from 4 to 12.5 mm over a thickness of 20 mm from one of the free edge of the plate. As $\lambda_{ZGV} \sim 8 \text{ mm}$, these holes are Mie scatterers in the vicinity of the ZGV-point. The ultrasound source consists in a 25 mm-length, 5 mm-width and 1 mm-thick piezoelectric strip glued on top of the plate [Fig. 2(b)]. This strip is located at 40 mm from the free edge and tilted 25° with respect to it. The width of the source ($\sim \lambda_{ZGV}/2$) allows to both excite the S_1 and S_{2b} Lamb modes in the vicinity of the ZGV-point. A $15 \mu\text{s}$ chirp signal spanning the frequency range $1.3 - 1.5 \text{ MHz}$ is sent to the transducer which generates an incident plane wave front. As previously, the out-of-plane component of the local vibration of the plate is measured with the photorefractive interferometer over an area of dimension $60 \times 120 \text{ mm}^2$. The wave field is recorded over a time length of 1 ms. In order to isolate the incident and reflected wave fronts in the vicinity of the ZGV-point, a discrete Fourier transform of the recorded signals is performed over overlapping time windows of 200

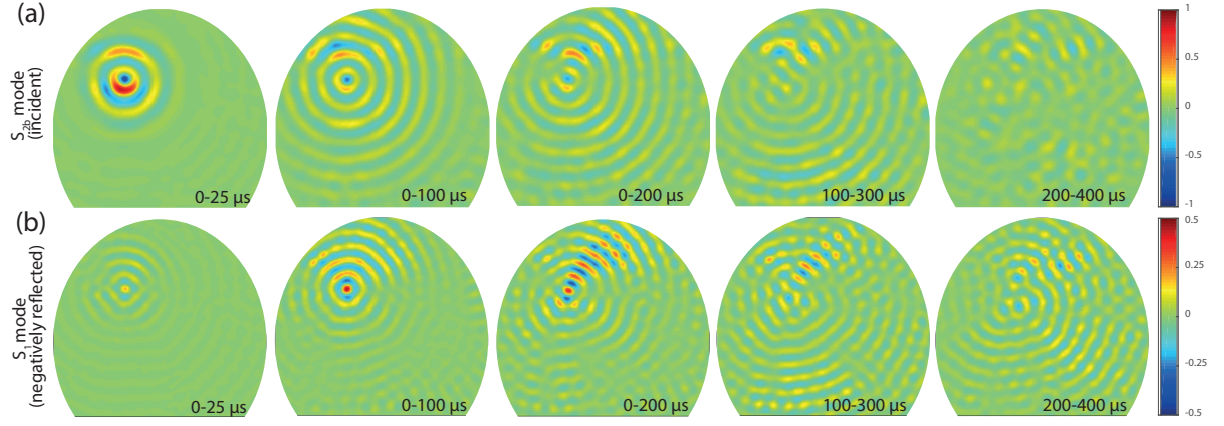


FIG. 4: Time evolution of the negative reflection process taking place in the truncated billiard. The S_{2b} and S_1 wave fields are displayed in panels (a) and (b), respectively, over the indicated time windows. Note also the different color scale in (a) and (b).

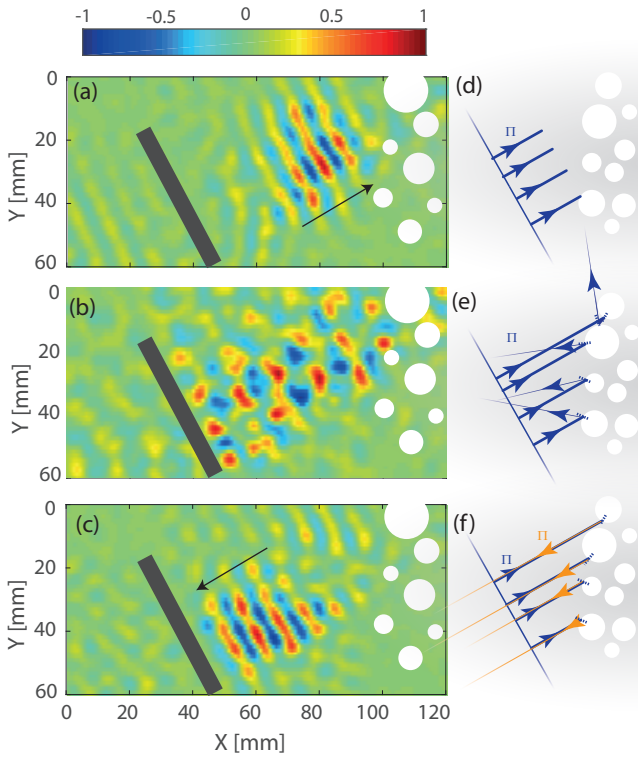


FIG. 5: Negative reflection in the disordered plate. (a) Incident wave field at frequency $f = 1.41$ MHz over the time widow 100-300 μ s. (b) Reflected wave field at frequency $f = 1.43$ MHz over the time widow 200-400 μ s. (c) NR wave field at frequency $f = 1.41$ MHz over the time widow 300-500 μ s. (d,e,f) Ray path trajectories involved in (a,b,c), respectively.

μ s. Figure 5(a) shows the incident wave front at time $t = 200$ μ s and frequency $f = 1.41$ MHz, *i.e.* in the vicinity of the ZGV frequency. This incident wave front is a wave packet of well-resolved momentum impinging the diffusive layer with an angle of incidence equal to 25° . This wave packet is then

scattered by the holes [Fig. 5(e,f)]. Figure 5(b) shows the reflected wave field at time $t = 300$ μ s and frequency $f = 1.43$ MHz. In this case, we are well above the ZGV-point displayed in Fig. 2(c). The wave number mismatch between the S_1 and S_{2b} modes implies a randomization of the reflected wave vector induced by the disordered layer [Fig. 5(e)]. This accounts for the speckle-like feature displayed by the reflected wave field in Fig. 5(b). On the contrary, in the vicinity of the ZGV frequency ($f = 1.41$ MHz), the incident and reflected wave vectors point exactly in opposite directions [see Fig. 5(f)]. Figure 5(c) shows the corresponding NR wave field at time $t = 400$ μ s and frequency $f = 1.41$ MHz. The dynamics of the NR process in the disordered slab is analyzed in more details in the Supplemental Material [38]. Despite disorder, NR gives rise to a well resolved wave packet with a momentum opposed to the incident one. The scattering layer retro-reflects the incident wave packet, as would the free edge of the plate. To some extent, the scattering layer is thus cloaked by the NR phenomenon. From a more practical point-of-view, this experiment illustrates how any scatterer can become a NR mirror that retro-reflects the incident wave field towards the source.

We have demonstrated the NR phenomenon with guided elastic waves in plates of arbitrary shape. Whatever the complexity of the plate, NR at its boundaries gives rise to a replica of the incident wave, following the same path but in a reverse way. NR displays focusing abilities similar to a phase conjugating mirror while being a fully passive process. On the one hand, negative reflection of elastic waves may find application in the development of new acoustic devices including resonators, lenses, and filters. On the other hand, this phenomenon can be extended to other fields of wave physics since, for instance, photonic crystals [23], chiral metamaterials [22] or graphene [24] can simultaneously support positive and negative phase velocity modes. Negative reflection can thus become a tool of choice for wave focusing applications in complex environments. The authors wish to thank T. W.

Murray for drawing our attention to the topic. The authors are grateful for funding provided by LABEX WIFI (Laboratory of Excellence within the French Program Investments for the Future, ANR-10-LABX-24 and ANR-10-IDEX-0001-02 PSL*) and by the Agence Nationale de la Recherche (ANR-15-CE24-0014-01, Research Project COPPOLA). B.G. acknowledges financial support from the French “Direction Générale de l’Armement” (DGA).

Supplementary Material

This document provides further information on the separation between the incident and negatively reflected components in the truncated billiard and the time evolution of the negative reflection process taking place in the disordered slab.

SEPARATION OF THE S_{2b} AND S_1 MODES IN THE TRUNCATED BILLIARD

Fig. S2(a) displays the wave-field recorded by the interferometric probe at frequency $f = 1.91$ MHz in the truncated billiard [see Fig. 2(a) of the accompanying paper]. Its spatial Fourier transform is displayed in Fig. S2(b). It exhibits two rings in the vicinity of $k_{ZGV} = 1.06 \text{ mm}^{-1}$. The inner ring is associated with the S_{2b} mode ($k_{2b} = 0.975 \text{ mm}^{-1}$) and the outer ring with the S_1 mode ($k_1 = 1.145 \text{ mm}^{-1}$). To separate both contributions, spatial low and high pass filters are applied with a cut-off at k_{ZGV} . Fig. S2(c) displays the result of the low pass filter in the spatial Fourier domain ($|k| < k_{ZGV}$). An inverse discrete Fourier transform (DFT) then yields the incident S_{2b} wave-field shown in Fig. 3(a) of the accompanying paper. Fig. S2(d) displays the result of the high pass filter in the spatial Fourier domain ($|k| > k_{ZGV}$). An inverse DFT then yields the negatively reflected S_1 wave-field shown in Fig. 3(c) of the accompanying paper.

Fig. S2(e) displays the wave-field recorded by the interferometric probe at frequency $f = 1.92$ MHz. Its spatial Fourier transform is displayed in Fig. S2(f). The inner ring is associated with the S_{2b} mode ($k_{2b} = 0.86 \text{ mm}^{-1}$) and the outer ring with the S_1 mode ($k_1 = 1.26 \text{ mm}^{-1}$). To separate both contributions, spatial low and high pass filters are applied with a cut-off at k_{ZGV} . Fig. S2(g) displays the result of the low pass filter in the spatial Fourier domain ($|k| < k_{ZGV}$). Fig. S2(h) displays the result of the high pass filter in the spatial Fourier domain ($|k| > k_{ZGV}$). Its inverse DFT then yields the reflected S_1 wave-field shown in Fig. 3(b) of the accompanying paper.

TIME EVOLUTION OF THE NEGATIVE REFLECTION PROCESS IN THE DISORDERED SLAB

The dynamics of the NR process in the disordered slab [see Fig. 2(b) of the accompanying paper] can be revealed by performing a DFT of the recorded signals over overlapping and apodized time windows of $200 \mu\text{s}$. The corresponding snapshots of the wave propagation versus time are displayed in Fig. S3 at frequency $f_{ZGV} = 1.41$ MHz. The wavefields at shorter times of flight ($t = 100 - 200 \mu\text{s}$) show the propagation of the incident wave packet towards the disordered slab. The wave-fields at longer times of flight ($t = 250 - 350 \mu\text{s}$) show the negatively reflected wave packet with a momentum anti-parallel to the incident wave vector.

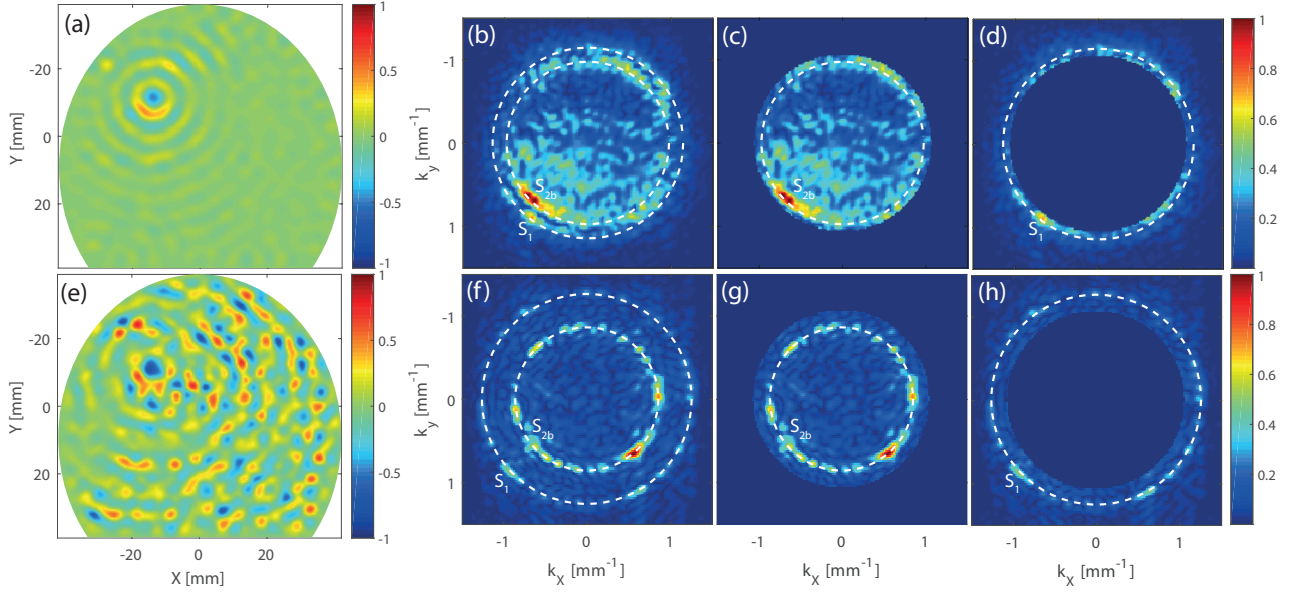


FIG. S2: (a) Recorded wave-field in the truncated billiard at frequency $f = 1.91$ MHz. (b) Spatial Fourier transform of the wave-field displayed in (a) at the zero-group velocity frequency $f_{ZGV} = 1.91$ MHz. (c) Low pass filter, $|k| < k_{ZGV}$, applied to the spatial Fourier transform of the wave-field in order to isolate the S_{2b} contribution at $f = 1.91$ MHz. (d) High pass filter, $|k| > k_{ZGV}$, applied to the spatial Fourier transform of the wave-field in order to isolate the S_1 contribution at $f = 1.91$ MHz. (e) Recorded wave-field at frequency $f = 1.92$ MHz. (f) Spatial Fourier transform of the wave-field displayed in (b) at $f = 1.92$ MHz. (g) Low pass filter, $|k| < k_{ZGV}$, applied to the spatial Fourier transform of the wave-field in order to isolate the S_{2b} contribution at $f = 1.92$ MHz. (h) High pass filter, $|k| > k_{ZGV}$, applied to the spatial Fourier transform of the wave-field in order to isolate the S_1 contribution at $f = 1.92$ MHz.

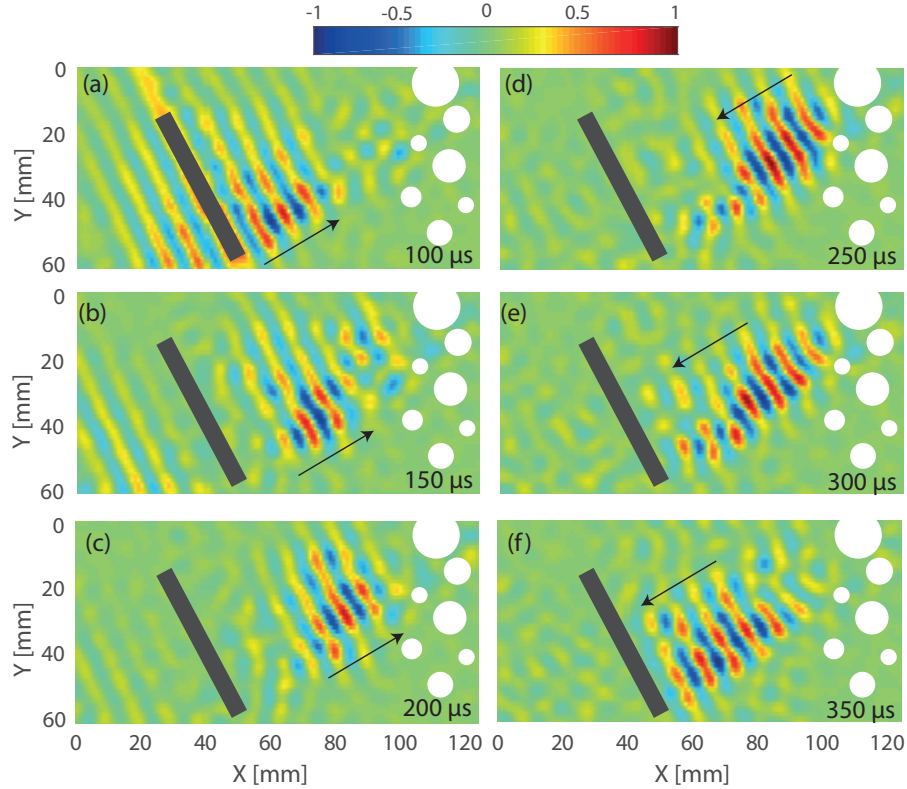


FIG. S3: Time evolution of the negative reflection process taking place in the disordered slab for different time windows of 200μ s-length. The indicated time corresponds to the center of the time window.

- ter, J.-L. Thomas, and F. Wu, Rep. Prog. Phys. **63** (2000).
- [2] G. Lerosey, J. de Rosny, A. Tourin, A. Derode, G. Montaldo, and M. Fink, Phys. Rev. Lett. **92** (2004).
- [3] V. Bacot, M. Labousse, A. Eddi, M. Fink, and E. Fort, Nature Phys. **12**, 972 (2016).
- [4] R. W. Hellwarth, J. Opt. Soc. Am. **67**, 1 (1977).
- [5] A. Yariv, IEEE J. Quant. Elect. **14**, 650 (1978).
- [6] R. Fisher, Optical Phase Conjugation (Academic Press, 1984).
- [7] A. Mosk, A. Lagendijk, G. Lerosey, and M. Fink, Nat. Photon. **6**, 283 (2012).
- [8] J. B. Pendry, A. J. Holden, D. J. Robbins, and W. J. Stewart, IEEE Trans. Microwave Theory Tech. **47**, 2075 (1999).
- [9] D. R. Smith, W. J. Padilla, D. C. Vier, S. C. Nemat-Nasser, and S. Schultz, Phys. Rev. Lett. **84**, 4184 (2000).
- [10] Z. Liu, X. Zhang, Y. Mao, Y. Y. Zhu, Z. Yang, C. T. Chan, and P. Sheng, Science **289**, 1734 (2000).
- [11] V. G. Veselago, Sov. Phys. Usp. **10**, 509 (1968).
- [12] J. B. Pendry, Phys. Rev. Lett. **85**, 3966 (2000).
- [13] R. A. Shelby, D. R. Smith, and S. Schultz, Science **292**, 77 (2001).
- [14] J. B. Pendry, D. Schurig, and D. R. Smith, Science **312**, 1780 (2006).
- [15] U. Leonhardt, Science **312**, 1777 (2006).
- [16] N. Yu and F. Capasso, Nature Mat. **13**, 139 (2014).
- [17] S. Maslovski and S. Tretyakov, J. Appl. Phys. **94**, 4241 (2003).
- [18] J. B. Pendry, Science **322**, 71 (2008).
- [19] A. Derode and M. Fink, Phys. Rev. Lett. **75**, 4206 (1995).
- [20] C. Draeger and M. Fink, Phys. Rev. Lett. **79**, 407 (1997).
- [21] J. B. Pendry, Science **306**, 1353 (2004).
- [22] C. Zhang and T. J. Cui, Appl. Phys. Lett. **91**, 194101 (2007).
- [23] Y. Sivan and J. B. Pendry, Phys. Rev. Lett. **106**, 193902 (2011).
- [24] V. V. Cheianov, V. Falko, and B. L. Altshuler, Science **315**, 1252 (2007).
- [25] B. Liu, W. Zhao, and Y. Jiang, Sci. Rep. **6**, 38314 (2016).
- [26] I. Tolstoy and E. Usdin, J. Acoust. Soc. Am. **29**, 37 (1957).
- [27] R. D. Mindlin, Structural Mechanics (Pergamon Press, New York, 1960), chap. Waves and vibrations in isotropic elastic plates, pp. 199–232.
- [28] A. H. Meitzler, J. Acoust. Soc. Am. **38**, 835 (1965).
- [29] K. Negishi, Jap. J. Appl. Phys. **26**, 171 (1987).
- [30] S. Bramhavar, C. Prada, A. A. Maznev, A. G. Every, T. B. Norris, and T. W. Murray, Phys. Rev. B. **83**, 014106 (2011).
- [31] F. D. Philippe, T. W. Murray, and C. Prada, Scient. Rep. **5**, 11112 (2015).
- [32] M. Germano, A. Alippi, A. Bettucci, and G. Mancuso, Phys. Rev. B. **85**, 012102 (2012).
- [33] I. A. Veres, C. Gr unsteidl, D. M. Stobbe, and T. W. Murray, Phys. Rev. B **93**, 174304 (2016).
- [34] B. G rardin, J. Laurent, C. Prada, and A. Aubry, J. Acoust. Soc. Am. **140**, 591 (2016).
- [35] D. Royer and E. Dieulesaint, Elastic Waves in Solid I (Springer Verlag, Berlin, 2000).
- [36] C. Prada, O. Balogun, and T. W. Murray, Appl. Phys. Lett. **87**, 194109 (2005).
- [37] S. D. Holland and D. E. Chimenti, Appl. Phys. Lett. **83**, 2704 (2003).
- [38] See Supplemental Material for further information on the separation between the incident and negatively reflected components of the wave field in the truncated billiard and the time evolution of the negative reflection process taking place in the disordered slab.